Hard Templating Pathways for the Synthesis of Nanostructured Porous Co_3O_4

Anja Rumplecker,[†] Freddy Kleitz,[‡] Elena-Lorena Salabas,[†] and Ferdi Schüth*[,†]

Max-Planck-Institut für Kohlenforschung, Kaiser-Wilhelm-Platz 1, D-45470 Mülheim an der Ruhr, Germany, and Department of Chemistry, Université Laval, Quebec G1K 7P4, Canada

Received May 8, 2006. Revised Manuscript Received September 29, 2006

The present study is concerned with the nanocasting preparation of Co_3O_4 nanostructures employing two-dimensional (2D) hexagonal SBA-15 and three-dimensional (3D) cubic KIT-6 as hard templates. The influence of framework connectivity of the parent silica and loading of the cobalt source are studied in detail. Structures can be tailored as isolated or randomly organized Co_3O_4 nanowires or as highly ordered mesoporous Co_3O_4 networks retaining the symmetry of the silica parent using 2D hexagonal parent materials. Applying cubic KIT-6 silica with suitable wall thickness and degree of framework interconnectivity as a template, we can vary the pore size of mesostructured Co_3O_4 from 3 nm up to values as high as 10 nm. To verify the influence of surface properties and texture, we employed different mesoporous silicas that were conventionally calcined at 550 °C and equivalent silica materials microwave treated in the presence of a concentrated H_2O_2/HNO_3 mixture. The parent silica materials and the resulting Co_3O_4 were characterized in detail at different steps during the templating route by nitrogen physisorption measurements and powder X-ray diffraction. Transmission electron microscopy and scanning electron microscopy investigations were performed to visualize the structure and morphology of the nanocast materials, and thermogravimetry−differential thermal analyses (TG−DTA) were done to follow the formation of Co_3O_4. With our method, preparation of nanocast Co_3O_4 is highly reproducible, regardless of template shapes and sizes, which makes the pathway much more versatile for a great variety of templates.

Introduction

Within the last years, different approaches have been reported concerning the preparation of nanostructured materials. For example, the top-down approach was proposed using various lithographic techniques using UV light or electron beams.[1] On the other hand, the bottom-up approach is based on molecular imprinting[2] or self-organization of liquid crystals, such as low-molecular-weight surfactants or block copolymers.[3] However, one limitation of these methods is that the resulting materials in most cases are lacking long-range order. Thus, the recently developed nanocasting strategy[4−6] seems to be a very attractive alternative. In this approach, pioneered by the group of Ryoo with the preparation of ordered mesoporous carbon (CMK-type family),[4,7,8] suitable precursors are incorporated in the pores and channels of highly ordered mesoporous silicas. After solidification is achieved within the pores, the parent silica materials may be selectively removed and shape-reversed molded structures can usually be obtained. One prominent example of such a siliceous porous mold used in the nanocasting route is the ordered mesoporous SBA-15 type silica.[9] SBA-15 material is generated under acidic conditions in the presence of triblock poly(ethylene oxide)−poly(propylene oxide)−poly(ethylene oxide) copolymers ($EO_nPO_mEO_n$) as structure-directing agents and exhibits well-ordered hexagonal arrays of large mesopores. Furthermore, in contrast to smaller pore MCM-41 silicas,[10] mesoporous silica synthesized with triblock copolymers as structure-directing agents generally contains additional porosity located inside the pore walls, originating from the interpenetration of silica and hydrophilic EO chains.[11−13] It was concluded that the presence of this interconnecting porosity is a prerequisite for a faithful and stable replication of the topology of the mesoporous silica hard templates.[14] In turn, the absence of bridging pores between the main channels of the parent silica materials leads to isolated nanowire systems during nanocasting.[7] Recently, the nanocasting approach was extended to allow the preparation of mesostructured metals and metal oxides of various

* Corresponding author. E-mail: shueth@mpi-muelheim.mpg.de.
[†] Max-Planck-Institut für Kohlenforschung.
[‡] Université Laval.

(1) Tennant, D. M. *Nanotechnology*; Timp, G., Ed.; Springer-Verlag: New York, 1998; p 161.
(2) Whitesides, G. M. *Sci. Am.* **1995**, *273*, 146.
(3) Muthukumar, M.; Ober, C. K.; Thomas, E. L. *Science* **1997**, *299*, 1225.
(4) Ryoo, R.; Joo, S. H.; Jun, S. *J. Phys. Chem. B* **1999**, *103*, 7743.
(5) Schüth, F. *Angew. Chem., Int. Ed.* **2003**, *42*, 3604.
(6) Feng, H. F.; Zhao, D. Y. *J. Mater. Chem.* **2005**, *15*, 1217.
(7) Ryoo, R.; Joo, S. H.; Kruk, M.; Jaroniec, M. *Adv. Mater.* **2001**, *13*, 677.
(8) Jun, S.; Joo, S. H.; Ryoo, R.; Kruk, M.; Jaroniec, M.; Liu, Z.; Ohsuna, T.; Terasaki, O. *J. Am. Chem. Soc.* **2000**, *122*, 10712.
(9) Zhao, D.; Huo, Q.; Feng, J.; Chmelka, B. F.; Stucky, G. D. *J. Am. Chem. Soc.* **1998**, *120*, 6024.
(10) Kresge, C. T.; Leonowicz, M. E.; Roth, W. J.; Vartuli, J. C.; Beck, J. S. *Nature* **1992**, *359*, 710.
(11) Imperor-Clerc, M.; Davidson, P.; Davidson, A. *J. Am. Chem. Soc.* **2000**, *12*, 898.
(12) Galarneau, A.; Cambon, H.; Di Renzo, F.; Ryoo, R.; Choi, M.; Fajula, F. *New J. Chem.* **2003**, *27*, 73.
(13) Soler-Illia, G. J. A. A.; Crepaldi, E. L.; Grosso, D.; Sanchez, C. *Curr. Opin. Colloid Interface Sci.* **2003**, *8*, 109.
(14) (a) Ryoo, R.; Ko, C. H.; Kruk, M.; Antoschuk, V.; Jaroniec, M. *J. Phys. Chem. B* **2000,** *104*, 11465. (b) Joo, S. H.; Ryoo, R.; Kruk, M.; Jaroniec, M. *J. Phys. Chem. B* **2002**, *106*, 4640.

10.1021/cm0610635 CCC: $37.00
Published on Web 01/11/2007

compositions, such as Pt[15−17] or Ag[18] and In_2O_3,[19−21] CeO_2,[22] Cr_2O_3,[20,23] Co_3O_4,[21,24] Fe_2O_3,[20] MgO,[25] or RuO_2[26], which are usually difficult to prepare by direct templating methods because of poor redox stability during template removal.[27,28] Further advantages of the nanocasting strategy to produce non-siliceous mesostructured materials have been reviewed in detail elsewhere.[4,6,29]

Despite the recent success in preparing a variety of nanostructured and mesoporous non-siliceous materials through the nanocasting strategy, it is often not clear what determines the properties of the replica structures; there is thus still an evident need for detailed investigations regarding the processes involved in material synthesis by nanocasting, particularly in the case of metal oxides. Further, the factors permitting efficient tailoring of texture and network topology remain to be determined. With regard to these aspects, we present in the following a comprehensive study of the synthesis of ordered mesoporous Co_3O_4 via the nanocasting route. Co_3O_4 is an important antiferromagnetic *p*-type semiconductor that can be widely used in electronic devices, as a sensor, and in magnetic heterostructures, but also as catalyst or as pigment.[30,34] The basic requirement for many of these applications is the preparation of structures not only reproducibly on the nanometer scale but also with a small distribution in size and tailored structural and textural properties.[31] Furthermore, we have recently reported a study of the magnetic properties of antiferomagnetic mesoporous Co_3O_4 nanostructures using superconducting quantum interference device (SQUID) magnetometry.[32] This recent study suggests specific magnetic properties of the nanostructured materials with the presence of an exchange interaction between the antiferromagnetic core and uncompensated spins on the surface.

With the goal of synthesizing new interesting materials, we demonstrate that it is possible to cast different mesoporous silica templates to form nanostructured Co_3O_4 spinels, using a simple nanocasting route. The pathway is highly reproducible, and can make use of silica templates having a wide range of structures, porosities and surface properties. The topology control of the nanocast Co_3O_4 materials will be examined in detail; accessible are nanostructured Co_3O_4 networks or isolated Co_3O_4 nanowires, with tunable structures, diameter, and domain size. Two types of ordered mesoporous silica were employed as hard templates: the two-dimensional (2D) hexagonal SBA-15[9,12,17] (*p*6*mm*) silica and the three-dimensional (3D) cubic KIT-6[33,34](*Ia*$\bar{3}$*d*). Among the known mesostructures, the cubic structure with the space group *Ia*$\bar{3}$*d* is one of the most interesting structures. Its pore network topology can be represented as an interpenetrating bicontinous network of channels. In contrast to materials with 2D hexagonal symmetry, the 3D cubic pore structure is highly branched and is highly accessible, making it an excellent template for the nanocasting approach. The pore size of mesostructured Co_3O_4 can be varied from 3 nm up to values as high as 10 nm, using cubic KIT-6 silica with suitable wall thickness and degree of framework interconnectivity. Additionally, the systematic investigations demonstrated that it is not necessary to use microwave-digested silica templates with high amounts of silanol functionalities on the wall surface[20] or vinyl-functionalized silica templates.[24] Using an optimized preparation method, the success of the method rather depends on the degree of interconnectivity of the parent silica materials and on loading effects.

Experimental Section

Materials. The nanostructured Co_3O_4 systems were prepared by hard templating from two-dimensional (2D) hexagonal SBA-15 silica and three-dimensionally (3D) ordered mesoporous silica exhibiting a cubic *Ia*$\bar{3}$*d* structure, also designated as KIT-6. Both silicas were either calcined at high temperatures (540−550 °C) or digested under microwave irradiation, in order to achieve different surface properties for comparison in the nanocasting. Calcined silica samples are designated as SBA-*x*-*y*-C, where *x* stands for the molar silica to surfactant ratio and *y* stands for the hydrothermal aging temperature applied during synthesis or as KIT-*y*-C, where *y* stands for the hydrothermal aging temperature applied during synthesis. Microwave-treated samples are designated SBA-*x*-*y*-MW. Co_3O_4 samples were designated Co-Hex-*y*-*z* and Co-Cubic-*y*-*z*, respectively, with *y* standing for the hydrothermal aging temperature of the parent silica and *z* standing for relative loading.

Synthesis of SBA-15 Silica. SBA-15 was prepared at low HCl concentration (0.3 M) in aqueous solution using tetraethoxysilane (TEOS, Acros 99%) as the silicon source and Pluronic P123 (EO_{20}-$PO_{70}EO_{20}$, Sigma-Aldrich) as a structure-directing agent. These synthesis conditions allow an easy and highly reproducible preparation of high quality SBA-15 material with high yields. In the synthesis of sample SBA-50-100-C1, 13.9 g of Pluronic P123 (EO_{20}-$PO_{70}EO_{20}$, Sigma-Aldrich) was dissolved in 252 g of distilled water and 7.7 g of HCl (37%). After complete dissolution, 25.0 g of TEOS was added at once. The mixture was left under stirring at 35 °C for 24 h, followed by a hydrothermal treatment at 100 °C for 24 h under static conditions. Reaction temperature of the samples SBA-

(15) Sakamoto, Y.; Ohsuna, T.; Hiraga, K.; Terasaki, O.; Ko, C. H.; Shin, H. J.; Ryoo, R. *Angew. Chem., Int. Ed.* **2000**, *39*, 3107.
(16) Shin, H. J.; Ko, C. H.; Ryoo, R. *J. Mater. Chem.* **2001**, *11*, 260.
(17) Choi, M.; Heo, W.; Kleitz, F.; Ryoo, R. *Chem. Commun.* **2003**, 1340.
(18) Han, Y.-J.; Kim, J. M.; Stucky, G. D. *Chem. Mater.* **2000**, *12*, 2068.
(19) Yang, H.; Shi, Q.; Tian, B.; Lu, Q.; Gao, F.; Xie, S.; Fan, J.; Yu, C.; Tu, B.; Zhao, D. *J. Am. Chem. Soc.* **2003**, *125*, 4724.
(20) (a) Tian, B. Z.; Liu, X. Y.; Yang, H. F.; Xie, S. H.; Yu, C. Z.; Tu, B.; Zhao, D. Y. *Adv. Mater.* **2003**, *15*, 1370. (b) Dickinson, C.; Zhou W.; Hodgkins, R. P.; Shi, Y.; Zhao, D. Y.; He, H. *Chem. Mater.* **2006**, *18*, 3088.
(21) Tian, B. Z.; Liu, X.; Solovyov, L.; Liu, Z.; Yang. H.; Zhang, Z.; Xie, S.; Zhang, F.; Tu, B.; Yu, C.; Terasaki, O.; Zhao, D. *J. Am. Chem. Soc.* **2004**, *126*, 865.
(22) Laha, S.; Ryoo, R. *Chem. Commun.* **2003**, 2138.
(23) Jiao, K.; Zhang, B.; Yue, B.; Ren, Y.; Liu, S.; Yan, S.; Dickinson, C.; Zhou, W.; He, H. *Chem. Commun.* **2005**, 5618.
(24) Wang, Y.; Yang, C. M., Schmidt, W.; Spliethoff, B.; Bill, E.; Schüth, F. *Adv. Mater.* **2005**, *17*, 53.
(25) Roggenbuck, J.; Tiemann, M. *J. Am. Chem. Soc.* **2005**, *127*, 1096.
(26) Shen, W.; Shi, J.; Chen, H.; Gu, J.; Zhu, Y.; Dong, X. *Chem. Lett.* **2005**, *34*, 390.
(27) Schüth, F. *Chem. Mater.* **2001**, *13*, 3184.
(28) Soler-Illia, G. J. A. A.; Sanchez, C.; Lebeau, B.; Patarin, J. *Chem. Rev.* **2002**, *102*, 4093.
(29) Lee, J.; Han, S.; Hyeon, T. *J. Mater. Chem.* **2004**, *14*, 478.
(30) (a) Wöllenstein, J.; Burgmair, M.; Plescher, G.; Sulima, T.; Hildenbrand, J.; Böttner, H.; Eisele, I. *Sens. Actuators, B* **2003**, *93*, 442. (b) Bahlawane, N.; Rivera, E. F.; Kohse-Höinghaus, K.; Brechling, A.; Kleineberg, U. *Appl. Catal., B* **2004**, *53*,245. (c) Makhlouf, S. A. *J. Magn. Magn. Mater.* **2002**, *246*, 184.
(31) *Nanoscale Materials in Chemistry*; Klabunde, K. J., Ed.; John Wiley and Sons: New York, 2001.
(32) Salabas, H. L.; Rumplecker, A.; Kleitz, F.; Radu, F.; Schüth, F. *Nano Lett.* **2006**, *6*, 2977.
(33) Kleitz, F.; Choi, S. H.; Ryoo, R. *Chem. Commun.* **2003**, 2136.
(34) Kim, T.-W.; Kleitz, F.; Paul, B.; Ryoo, R. *J. Am. Chem. Soc.* **2005**, *127*, 7601.

50-100-C2 and SBA-50-100-MW was 40 °C. The solid product was filtered without washing and dried for 48 h at 95 °C. It was proposed by Choi et al.[17] that the pore connectivity of SBA-15 could be modified by adjusting the silica to surfactant ratio. To do that, we prepared a set of samples according to the conditions used for the standard procedure described above (SBA-50-100-C1), with the difference of variation in the molar ratio of silica to surfactant ($r = 45-60$). Accordingly, TEOS amounts ranging from 22.5 to 29.8 g were used. In another set of experiments, the hydrothermal treatment temperature under static conditions, following the initial reaction at 35 °C, was varied from 50 to 100 °C. For most of the conditions, several batches of materials have been prepared, with textural parameters (pore volume, surface area) typically scattering within ±10%.

Synthesis of KIT-6 Silica. Large quantities of high quality mesoporous cubic $Ia\bar{3}d$ silica material are easily obtained following the method reported by Kleitz et al.[33] KIT-6 was prepared at a low HCl concentration (0.5 M) in an aqueous solution using tetraethoxysilane (TEOS, Acros 99%) as the silicon source and a blend of Pluronic P123 and *n*-butanol (Aldrich, 99%) as a structure-directing mixture. Briefly, 9 g of Pluronic P123 was dissolved in 325 g of distilled water and 17.4 g of HCl (37%) under vigorous stirring. After complete dissolution, 9 g of butanol was added. The mixture was left stirring at 35 °C for 1 h, after which 19.35 g of TEOS was added at once to the homogeneous clear solution. This mixture was further left stirring at 35 °C for 24 h, followed by aging at 100 °C for 24 h under static conditions (this process is referred to as hydrothermal treatment). The solid product was filtered without washing and dried for 48 h at 95 °C. In another set of experiments, the hydrothermal treatment temperature under static conditions, following the initial reaction at 35 °C, was varied from 35 to 130 °C. To check reproducibility, the synthesis of several batches was repeated, with negligible scatter of the properties of the resulting materials.

Removal of the Copolymer Template. After the synthesis, the dried SBA-15 and KIT-6 samples were split in two fractions to remove the Pluronic P123 template either by calcination or microwave digestion. For the calcination procedure, the as-synthesized silica powder was first shortly slurried in an ethanol−HCl mixture, filtered, dried, and subsequently calcined at 550 °C. To remove the organic template and generate high concentrations of silanol surface groups, we treated the other fractions of as-synthesized SBA-15 and KIT-6 templates under microwave irradiation.[35] A typical microwave digestion is as follows: 0.6 g of dried as-synthesized silica (SBA-15 or KIT-6) powder are placed in a Teflon autoclave, to which a mixture of 4 mL of HNO_3 (15 M, 65%) and 2 mL of H_2O_2 (30%) (premixed) is then added. The mixture is then exposed to microwave irradiation for 15 min under static conditions at 150 °C. The heating time up to 150 °C is 2 min and the power input is set to 1200 W. After being cooled, the solid is filtered and washed extensively with ethanol. The resulting white powder is dried overnight at room temperature and for 3−4 h more at 80 °C.

Nanocasting Preparation of Co_3O_4. Nanostructured Co_3O_4 samples were prepared using calcined 2D hexagonal SBA-15 or calcined 3D cubic KIT-6 of different degrees of interconnectivity and different diameters as the host. Typically, in a polypropylene (PP) vessel, 0.2 g of SBA-15 were dispersed in 2 mL of a 0.8 M solution of $Co(NO_3)_2{\cdot}6H_2O$ (Fluka) in ethanol and stirred at room temperature for 1 h. Ethanol was removed by evaporation by heating the PP vessel overnight at 80 °C. Afterward, the resulting powder of pink color was heated in a ceramic crucible in an oven at 200 °C for 10 h to completely decompose the nitrate species. The impregnation and decomposition steps were repeated twice following the same conditions in order to achieve higher loadings. The resulting material was calcined at 450 °C for 6 h. The silica template was then removed at room temperature using a 2 M NaOH aqueous solution. The NaOH etching of silica was repeated 4 times, each time using a fresh NaOH solution (5 mL). The black Co_3O_4 material was recovered by centrifugation and finally dried at 50 °C. The influence of inorganic precursor loading (15, 18, and 24%) was examined using the silica template SBA-50-100-C1. Considering the density of Co_3O_4 and the pore volume of the parent silicas, relative loadings were determined according to the molar amount of Co_3O_4 within the pore system after decomposition of the nitrate precursor.

For size variation, 2D hexagonal SBA-15 and 3D cubic KIT-6 samples of different pore diameters were used as silica templates. For these samples, identical relative loadings of Co_3O_4 in the Co_3O_4/silica composite were adjusted according to the total pore volume of the parent silica.

Alternatively, nanostructured Co_3O_4 materials were prepared using the microwave digested large pore silica. The method is adapted to the one proposed by Zhao et al.[21] Typically, 0.15 g of microwave digested mesoporous silica was dispersed in 5 mL of ethanol, after which 0.408 g (1.4 mmol) of $Co(NO_3)_2{\cdot}6H_2O$ (Fluka) was added at once. This mixture was left for 90 min under stirring at room temperature. The mixture was then carefully transferred to a flat petri dish and dried overnight at 40 °C to evaporate the solvent. The resulting powder of pink color was subsequently calcined at 350 °C for 5 h (with an intermediate plateau at 170 °C for 2 h to decompose the nitrate). Afterward, the same impregnation step was repeated with 0.175 g (0.6 mmol) of $Co(NO_3)_2{\cdot}6H_2O$ added to the black powder dispersed in 5 mL of ethanol. After overnight evaporation of the solvent, the second calcination was performed at 550 °C for 5 h, with the same intermediate step of 2 h at 170 °C. The silica template was removed at room temperature using a 2 M NaOH aqueous solution. The NaOH etching of silica was repeated four times, each time using a fresh NaOH solution (5 mL). The Co_3O_4 materials were recovered by centrifugation, washed with water and finally dried at 50 °C. Reproducibility was checked by repeating the syntheses of several batches.

Characterization. The quality of 2D hexagonal SBA-15 and 3D cubic KIT-6 was checked by low-angle X-ray diffraction (XRD) recorded on a Stoe diffractometer operating in reflection mode with Cu Kα radiation. The step width was 0.02° at an acquisition time of 8−10 s per step. The mesostructures of the nanocast Co_3O_4 samples were analyzed using a step width of 0.01° at an acquisition time of 40−60 s per step. Using wide angle XRD, the pure Co_3O_4 spinel phase was verified after calcination and after NaOH etching.

High-resolution transmission electron microscopy (HRTEM) images were obtained on a Hitachi HF2000 microscope with a cold field emitter operated at 200 kV. Scanning electron microscopy (SEM) and energy dispersive X-ray analysis (EDX) were conducted on a Hitachi S-3500N. Nitrogen physisorption experiments were measured on a Micromeritics ASAP 2010 system at liquid nitrogen temperature (−196 °C) with prior degassing of the calcined silica samples under vacuum at 200 °C, microwave-digested samples at 150 °C, and nanocast Co_3O_4 at 150 °C overnight. Total pore volumes were determined using the adsorbed volume at a relative pressure of 0.97. Multipoint Brunauer−Emmet−Teller (BET)[36] surface area was estimated from the relative pressure range from 0.05 to 0.2. The pore size distribution of the mesoporous materials was analyzed using both the Barrett−Joyner−Halenda (BJH)

(35) Tian, B.; Liu, X.; Yu, C.; Gao, F.; Luo, Q.; Xie, S.; Tu, B.; Zhao, D. *Chem. Commun.* **2002**, 1186.

(36) Brunauer, S.; Emmet, P. H.; Teller, E. *J. Am. Chem. Soc* **1938**, *60*, 309.

algorithm[37] and for the silica materials additionally using non-local density functional theory (NLDFT) methods.[38,39] For the DFT analyses, the Autosorb-1 software supplied by Quantachrome Instruments was used. The kernel of NLDFT equilibrium capillary condensation isotherms of N_2 at −196 °C on silica was selected for the model isotherms, using the desorption branch and assuming cylindrical pores.

Thermal decomposition (TG−DTA) of cobalt nitrate was investigated using a Netzsch STA 449C thermal analyzer over a temperature range from room temperature to 600 °C. The measurements were carried out in a flow of air at a heating rate of 1 °C/min. For comparison, the pure $Co(NO_3)_2 \cdot 6H_2O$, SBA-50-100-C1, impregnated with an 0.8 M cobalt nitrate solution, and pure $Co(NO_3)_2 \cdot 6H_2O$ mixed with Aerosil and SBA-15, respectively, were also measured.

Results and Discussion

The few previous reports on the synthesis of Co_3O_4 suggested that successful incorporation of cobalt oxide precursor solutions inside mesoporous silica during the nanocasting process may be restricted to silica templates with specific surface properties. For instance, Zhao et al.[20,21] reported the preparation of various metal oxides, including Co_3O_4, via nanocasting using mesostructured silica templates exposed to microwave digestion. The microwave digested silica materials described therein are characterized by a high density of silanol groups present on the pore wall surface. The presence of a high density of Si−OH was thought to be beneficial for the homogeneous incorporation of large amounts of metal salts inside mesoporous silica. On the other hand, it was recently reported by Wang et al. that replication to form Co_3O_4 would also be facilitated using silica templates with vinyl-functionalized pore surface.[24] There, it was reported that no ordered cobalt oxide could be obtained when a pure silica material was used as a template. However, recent reports on other metal oxides prepared within the pores of mesoporous silica do not emphasize the need for a particular surface treatment.[22,23,26]

To verify the influence of surface properties and texture, we used different mesoporous silicas that were either conventionally calcined at 550 °C[40] or microwave-treated in the presence of a concentrated H_2O_2/HNO_3 mixture.[35] The nitrogen physisorption isotherms measured for SBA-15 calcined at 550 °C (SBA-50-100-C2) and SBA-15 microwave-digested at 150 °C (SBA-50-100-MW) are shown in Figure 1. Corresponding X-ray diffraction patterns can be found in the Supporting Information (Figure S1).

Both mesoporous silicas are derived from the same as-synthesized SBA-15 material, prepared at 35 °C using 0.3 M HCl, with subsequent aging performed at 100 °C. Clearly, the hysteresis loop observed for the microwave-digested sample (SBA-50-100-MW) occurs at much higher relative pressures than that of the calcined equivalent, indicating much larger mesopore dimensions. The larger mesopore

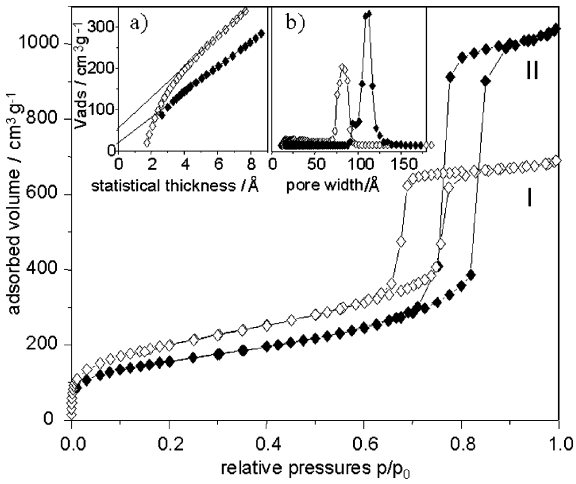

Figure 1. Nitrogen physisorption isotherms of calcined SBA-15 (I, SBA-50-100-C2) and microwave digested SBA-15 (II, SBA-50-100-MW). The insets are (a) *t*-plot, and (b) pore size distributions calculated from the DFT method.

dimension is also substantiated by the pore size distributions calculated by the density functional theory (DFT) method (Figure 1, inset). Furthermore, the pronounced capillary condensation step observed for SBA-50-100-MW points to significantly larger mesopore volume compared to the calcined sample SBA-50-100-C. Considering the *t*-plots, SBA-50-100-MW seems to possess a smaller micropore volume than calcined SBA-15. Also, the pore size distribution calculated by DFT suggests that there are no pores smaller than 2 nm for SBA-50-100-MW, whereas SBA-50-100-C2 has a substantial fraction of micropores. As will be shown below, a complementary porosity resulting in framework interconnection is nevertheless also present in SBA-50-100-MW. Here, one could speculate that the bridging pores present in SBA-50-100-MW are of much larger dimension and, thus, might mainly contribute to the mesoporosity of the materials.[41,42] Similar observations were made for the cubic KIT-6 silica template when comparing calcination and microwave treatment (see the Supporting Information, Figure S2). Size variation of both silica templates was achieved by varying the temperature of hydrothermal treatment. For systematic studies, the silica to copolymer ratio was kept constant, even though it was known from platinum replication that variation of the silica to copolymer ratio could also affect the bridging interconnectivity of the mesopores.[17]

Figure 2 clearly illustrates the influence of the temperature of the hydrothermal treatment on pore dimensions for the case of the cubic $Ia\bar{3}d$ phase. Relative pressures at which the hysteresis loop for a specific sample occurs decrease with decreasing temperature of hydrothermal treatment, indicating the decreasing pore dimensions. Additionally, for samples hydrothermally treated at higher temperatures (KIT-100-C, KIT-135-C), a pronounced capillary condensation step was observed, which reflects large pore volumes. Pore volumes of the samples strongly depend on this thermal treatment, so that KIT-40-C (0.4 $cm^3\ g^{-1}$) has a pore volume of only about one-third of that of KIT-135-C (1.3 $cm^3\ g^{-1}$). It should

(37) Barret, E. P.; Joyner, L. G.; Halenda, P. P. *J. Am. Chem. Soc.* **1951**, *73*, 373.
(38) Ravikovitch, P. I.; Domhnaill, S. C. O.; Neimark, A. V.; Schüth, F.; Unger, K. *Langmuir* **1995**, *11*, 4765.
(39) Ravikovitch, P. I.; Neimark, A. V. *J. Phys. Chem. B* **2001**, *105*, 6817.
(40) Kleitz, F.; Schmidt, W.; Schüth, F. *Microporous Mesoporous Mater.* **2003**, *65*, 1.
(41) Yates, T. J. V.; Thomas, J. M.; Ferdandez, J. J.; Terasaki, O.; Ryoo, R.; Midgley, P. A. *Chem. Phys. Lett.* **2006**, *418*, 540.
(42) Kleitz, F.; Thommes, M. **2006**, unpublished results.

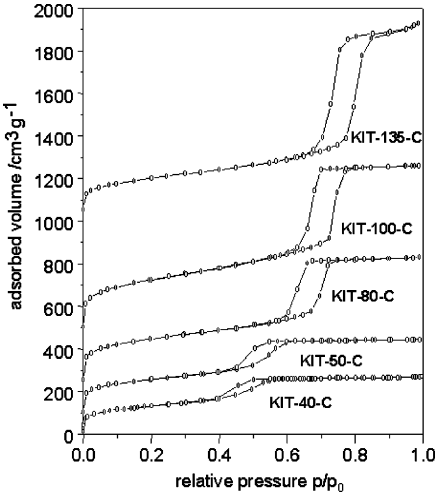

Figure 2. Nitrogen physisorption for calcined KIT-6 prepared at different hydrothermal treatment temperatures; for clarification, the data are given with an offset of 100 $cm^3\ g^{-1}$ (KIT-50-C), 250 $cm^3\ g^{-1}$ (KIT-80-C), 500 $cm^3\ g^{-1}$ (KIT-100-C), and 1050 $cm^3\ g^{-1}$ (KIT-135-C).

Table 1. Structural Parameters of 2D Hexagonal Mesoporous SBA-15 Silica Templates[a]

silica template	SiO_2/P123	T (°C)	S_{BET} ($m^2\,g^{-1}$)	V_T ($cm^3\,g^{-1}$)	d_0 (nm)	a_0 (nm)	h_w (nm)
SBA-50-50-C	50	50	655	0.99	3.8	8.85	5.0
SBA-50-80-C	50	80	702	0.96	4.4	9.61	5.2
SBA-50-100-C1	50	100	897	1.2	5.8	11.0	5.2
SBA-60-100-C	60	100	709	0.8	5.1	10.0	4.9
SBA-50-100-C2	50	100	777	1.1	6.5	11.5	5.0
SBA-50-100-MW	50	100	565	1.6	9.0	13.2	4.2

[a] S_{BET} is the specific surface area deduced from the isotherm analysis in the relative pressure range of 0.05−0.2; V_T is the total pore volume at relative pressures 0.95; d_0 is the pore diameter calculated from the desorption branch of the isotherm using the BJH method; XRD unit-cell parameter a_0 is equal to $2d_{100}/3^{1/2}$; the wall thickness $h_w = a_0 - d_0$.

Table 2. Structural Parameters of 3D Cubic Mesoporous KIT-6 Silica Templates[a]

silica template	T (°C)	S_{BET} ($m^2\,g^{-1}$)	V_T ($cm^3\,g^{-1}$)	d_0 (nm)	a_0 (nm)	h_w (nm)
KIT-40-C	40	471	0.4	3.4	18.7	6.0
KIT-50-C	50	533	0.5	3.9	19.7	5.9
KIT-80-C	80	677	0.9	5.9	21.6	4.9
KIT-100-C	100	782	1.1	6.4	22.8	5.0
KIT-135-C	135	543	1.3	8.3	24.0	3.7

[a] XRD unit-cell parameter a_0 is equal to $6^{1/2}d_{211}$; the wall thickness $h_w = a_0/2 - d_0$.

be noted here that for successful replication, the exact pore volume has to be known, because loading with cobalt oxide precursor has to be adjusted accordingly. Nitrogen physisorption isotherms of calcined SBA-15 samples as a function of temperature of hydrothermal treatment are given in Figure S3 of the Supporting Information.

Tables 1 and 2 summarize the physicochemical parameters of the different SBA-15 and KIT-6 silica templates, respectively. The values are absolutely consistent with previous data obtained for such high-quality SBA-15 materials.[12] The obtained BET surface areas, pore volumes, wall thicknesses, and interconnectivity of the silica are influenced by the aging temperature. The wall thickness of the material was calculated using the pore size obtained from N_2 sorption data using the BJH method and the unit-cell parameter a_0 from X-ray diffraction, as described previously.[43] From Tables 1 and 2, it can be seen that for KIT-6, the wall thickness is increasing with decreasing temperature of hydrothermal treatment, whereas it is almost unaffected for SBA-15. BET surface area and pore volumes for the cubic KIT-6 phases are in line with previous results.[34] The materials are obtained in high yields and high quality.

In the following, the use of the above-described KIT-6 and SBA-15 samples as templates for the preparation of nanostructured Co_3O_4 spinels will be described. In a general preparation procedure of nanocast Co_3O_4, 2D hexagonal SBA-15 or 3D cubic KIT-6 templates are impregnated with a solution of cobalt nitrate in ethanol, calcined, and eventually re-impregnated in order to maximize the loading with inorganic precursor. To recover the mesoscaled Co_3O_4, we dissolved the parent silica templates with a 2 M NaOH solution. The remaining materials consist of ordered or disordered nanowire arrays in the case of SBA-15 templates and nanostructured networks in the case of KIT-6 templates. In case of high interconnectivity of the hard templates, these arrays reflect the pore topology of the parent material.

In a typical synthesis, we disperse a defined amount of SBA-15 in a solution of cobalt nitrate in ethanol in a polypropylene (PP) vessel at room temperature for 1 h. In comparison to the use of glass containers, nanocast cobalt oxide of higher quality was obtained at high loadings if the materials were prepared with vessels having hydrophobic surfaces as PP. This may be due to the fact that a hydrophobic vessel surface leads to favored penetration of the liquid into the pore system of the mold and less remaining liquid on the external surface of the powder.

After a first calcination at 200 °C, the obtained Co_3O_4/silica composite material was analyzed using nitrogen sorption and powder X-ray diffraction (XRD). Wide-angle XRD shows that treatment at this low temperature already leads to the formation of the Co_3O_4 structure (see the Supporting Information, Figure S4). The cobalt oxide formation is accompanied by a large density increase, with the result that a part of the pore system then becomes accessible again. To achieve higher loadings of the cobalt oxide precursor, we repeated the impregnation step until a maximum loading was reached. Pore filling of the silica by the cobalt oxide was monitored with nitrogen physisorption measurements performed after each step of impregnation (Figure 3).

In this paper, loading values are given as volume percent of the accessible pore volume filled with Co_3O_4, assuming the bulk density of Co_3O_4 for the cobalt oxide in the pore system. To compare silica samples with different porosity, we did not impregnate parent silicas with identical absolute $Co(NO_3)_2{\cdot}6H_2O$ loading but with identical relative filling of Co_3O_4 in the pore systems. To optimize loadings of Co_3O_4 in the parent silica in a smaller number of steps, we attempted to increase the amount of cobalt incorporated by using cobalt nitrate precursor solutions with higher concentrations of 1.6 and 3.2 mol L^{-1} (Figure 3). However, TEM analysis showed that this led to the formation of bulk cobalt oxide particles

(43) Solovyov, L. A.; Zaikovskii, V. I.; Shmakov, A. N.; Belousov, O. V.; Ryoo, R. *J. Phys. Chem. B* **2002**, *106*, 12198.

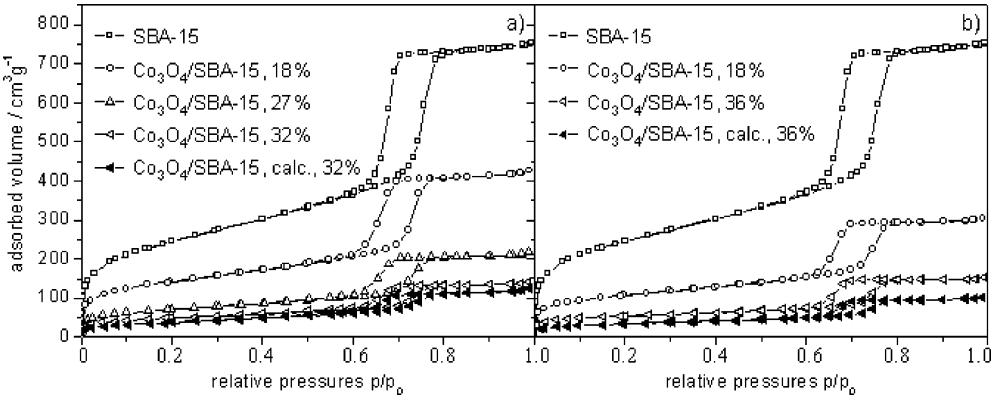

Figure 3. Pore filling of SBA-50-100-C and intermediate steps of the composite Co_3O_4/SBA-15, final loading Co_3O_4/SBA-15 after calcination for a maximum loading of (a) 32% in three impregnation steps and (b) 36% in two impregnation steps using precursor solutions with higher concentrations.

outside of the pores of silica. Therefore, for all experiments reported here, the standard concentration of 0.8 mol L^{-1} was used. In Figure 3, one notes a stronger reduction of the accessible pore volume than would be expected from the loadings. This can be attributed to parts of the pore system being blocked by the presence of cobalt oxide in the pores, because up to loadings of about 30%, no externally grown cobalt oxide could be detected by TEM.

For nanocasting to be successful, the precursors should be decomposed thermally inside the pores to give the desired phase. To produce homogeneous materials, possible decomposition products should leave the samples preferentially via the gas phase. For these reasons, acetates or nitrates are used as precursors in order to produce high-surface-area materials. One possible drawback of the nanocasting approach is the risk of pore blocking. Pore blocking would lead to low loadings and, therefore, to low product yields and possibly materials of poor quality. Another implication of pore blocking is the risk of formation of bulk particles outside the hard template. Such particles would not be nanostructured and may grow even further during calcination at elevated temperatures. Hence, the choice of the precursor, the impregnation technique, and the appropriate heat treatment are of high relevance for nanocasting.

Thermal decomposition of cobalt nitrate compounds had been studied by Brockner et al. to prepare anhydrous cobalt (II) nitrate.[44] However, the pore system and the presence of the silica may affect the decomposition, and therefore these data are not necessarily directly transferable. To elucidate the complete decomposition process of metal nitrates inside the pore system of mesoporous silica, TG−DTA experiments were performed. The results for pure cobalt nitrate hexahydrate, cobalt nitrate hexahydrate mixed with calcined SBA-15, cobalt nitrate hexahydrate mixed with Aerosil 380 silica, and cobalt nitrate hexahydrate impregnated inside the pores of calcined SBA-15 (SBA-50−100-C1) are depicted in Figure 4. All samples contain almost identical absolute amounts of cobalt nitrate hexahydrate; therefore absolute mass loss is given in the figure to allow direct comparison.

For all samples, several inflection points of the weight loss curve and the DTA curve indicate a stepwise decomposition. The first inflection point of the well-resolved DTA curve of pure $Co(NO_3)_2{\cdot}6H_2O$ represents the endothermic loss of excess water followed by release of the first two molecules of crystal water at 80 °C. Further heating leads to the loss of the next two pairs of water molecules at 120 and 150 °C. The decomposition of the nitrate takes place above 210 °C for the pure $Co(NO_3)_2{\cdot}6H_2O$. All these processes are accompanied by a strong weight loss as recorded in the TG plot. The measured decomposition temperatures and mass losses for the measurement of pure $Co(NO_3)_2{\cdot}6H_2O$ are compiled in Table 3.

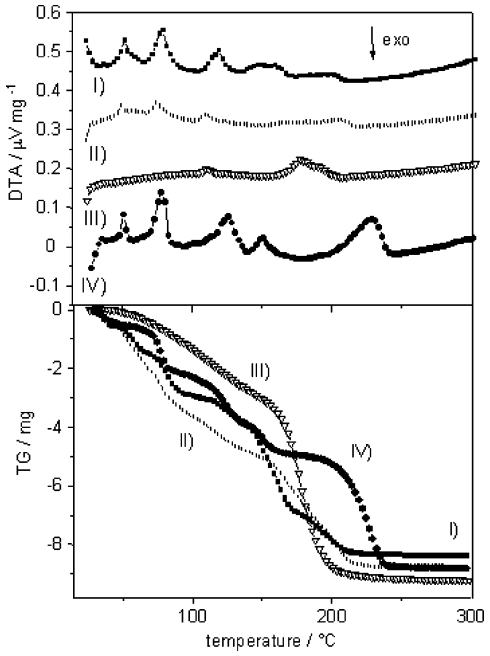

Figure 4. DTA and TG results. For clarity, DTA measurements are plotted with the offset given in parentheses; $Co(NO_3)_2{\cdot}6H_2O$ ground with Aerosil 380 (I, 0.45 μV mg^{-1}), $Co(NO_3)_2{\cdot}6H_2O$ ground with SBA-15 (II, 0.3 μV mg^{-1}), $Co(NO_3)_2{\cdot}6H_2O$ impregnated on SBA-15 (III, 0.15 μV mg^{-1}), and pure $Co(NO_3)_2{\cdot}6H_2O$ (IV).

Table 3. Steps of Thermal Decomposition from TG−DTA Measurements of the Pure $Co(NO_3)_2{\cdot}6H_2O$ Sample (absolute losses for 12.5 mg of starting material as used in experiments)

decomposition	T (°C)	Δm (%)	Δm/mg
$Co(NO_3)_2{\cdot}6H_2O \rightarrow Co(NO_3)_2{\cdot}4H_2O + 2H_2O$	80	12.8	1.67
$Co(NO_3)_2{\cdot}4H_2O \rightarrow Co(NO_3)_2{\cdot}2H_2O + 2H_2O$	120	13.2	1.74
$Co(NO_3)_2{\cdot}2H_2O \rightarrow Co(NO_3)_2 + 2H_2O$	150	10.9	1.01
$3\,Co(NO_3)_2 \rightarrow Co_3O_4 + N_2O_4 + 2N_2O_5$	>210	31.4	3.92

(44) Ehrhard, C.; Gjikaj, M.; Brockner, W. *Thermochim. Acta.* **2005**, *432*, 36.

For the $Co(NO_3)_2 \cdot 6H_2O$ mixed together with SBA-15 and Aerosil 380, respectively, the release of excess water and the first decomposition step take place at the same temperature as for the pure $Co(NO_3)_2 \cdot 6H_2O$. On the other hand, for both samples, a shift in the oxide formation was observed toward lower temperatures. All measurements indicate that a silica surface does not influence the temperature of dehydration of the hexahydrates, but clearly lowers the temperature of the oxide formation. This may be explained by a kinetic acceleration of the decomposition of smaller crystals on a support, but other influences, such as energetically favorable interaction of the formed oxide with the silica, cannot be excluded. For the SBA-15 sample, the decomposition steps are not well-resolved in mass loss and in the DTA signal. This is probably due to the delayed release of the decomposition products from the interior of the pore system.

All Co_3O_4 samples were analyzed with TEM, SEM, EDX, nitrogen physisorption, and wide- and low-angle XRD measurements. The effect of loading on the size of the ordered domains and on the overall particle morphology was investigated using SBA-15 as the mold. Therefore, calcined SBA-15 (SBA-50-100-C1) was impregnated with a solution of cobalt nitrate in ethanol stepwise until loadings of 15, 18, and 24% Co_3O_4 relative to the total pore volume of SBA-50-100-C1 (1.2 cm^3g^{-1}) were achieved. For example, in the case of sample Co-Hex-100-24, 5.2 mL of a 0.8 M cobalt nitrate solution was added to 200 mg of SBA-50-100-C1 in three steps of impregnation, which corresponds to 21 mmol $Co(NO_3)_2 \cdot 6H_2O$ per g of silica. With the bulk density of Co_3O_4 (6.11 g cm^{-3}), the complete filling of the accessible pore volume would correspond to 30.6 mmol Co_3O_4 per g. Because of a large mass loss during decomposition of the nitrate precursor, a complete filling of the pore with Co_3O_4 is not feasible. However, it is interesting to know the threshold filling from which externally deposited Co_3O_4 particles are produced.

TEM images of the obtained Co_3O_4 materials after NaOH etching are shown in Figure 5. In all three cases, nanowires of Co_3O_4 were observed with a diameter of 7 nm. The parent silica SBA-50-100-C1 consists of mesopores with a diameter of 5.8 nm, determined using the BJH algorithm from the desorption branch of the nitrogen physisorption isotherm; this value is in reasonable agreement with the wire diameter, considering the uncertainties both in the determination of the pore size and the exact determination of the wire diameters in the TEM.[39]

The TEM images clearly show the dependence of the order of the resulting cobalt oxide on the loading of the silica. At low loadings, disordered arrangements of nanowires (average length around 70 nm) are obtained; for higher loadings (Co-Hex-100-24), large bundles of mesostructured Co_3O_4 nanowires are observed. The nanowires forming the arrays are separated by a constant repeat distance, corresponding to the wall thickness of the parent SBA-15. In contrast to that, in Co-Hex-100-15, such a uniform repeat distance of the Co_3O_4 nanowires is not present. Therefore, already the TEM analysis reveals that the loading strongly influences interconnectivity of Co_3O_4 nanowires. The structure can be tuned from randomly packed, isolated Co_3O_4 nanowires to highly ordered, mesostructured, and fully interconnected networks possessing the same symmetry as the parent silica material. For calcined materials, a critical relative loading of around 17% seems to be necessary to obtain materials reflecting the 2D hexagonal symmetry of the parent silica.

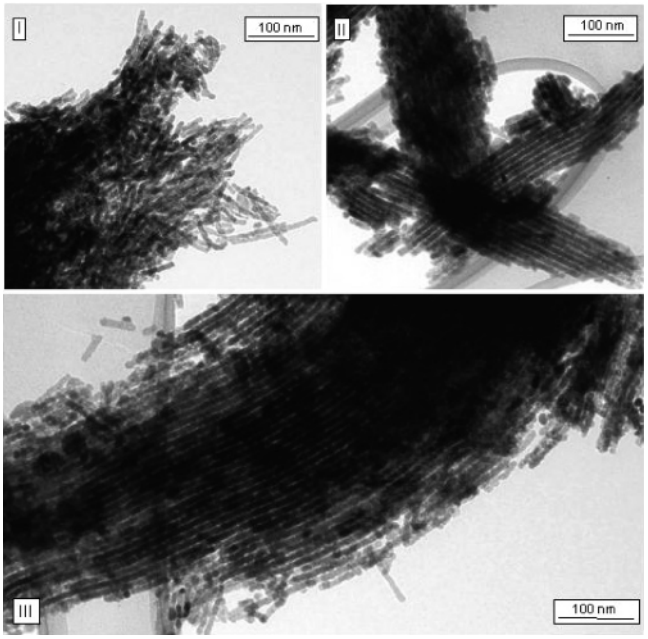

Figure 5. Interconnectivity and mesostructured ordered domain size. TEM images of nanocast Co_3O_4 depending on loading: (I) Co-Hex-100-15, (II) Co-Hex-100-18, and (III) Co-Hex-100-24 (silica template: SBA-50-100-C1).

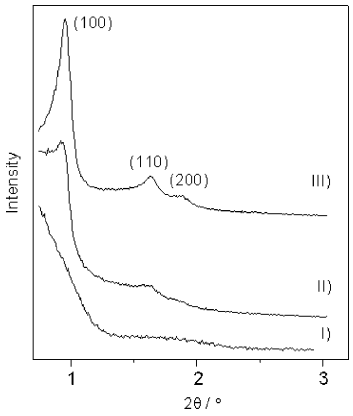

Figure 6. Low-angle XRD of nanocast Co_3O_4 for three samples obtained at different loadings: (I) Co-Hex-100-15, (II) Co-Hex-100-18, and (III) Co-Hex-100-24.

Figure 6 shows the low-angle XRD patterns of the pure Co_3O_4 samples after dissolution of the silica. The low angle regions show the characteristic reflections of the 2D hexagonal *p6mm* structure only for the samples above this loading value (Figure 6, II and III). Co-Hex-100-18 and Co-Hex-100-24 consist of significantly larger ordered domains. With increasing loading, the appearance of the characteristic mesostructure reflections and their narrowing indicate the substantial increase in the size of the ordered domains. As seen in Figure 6, the symmetry corresponds to the parent SBA-15 (SBA-50-100-C1), with even the higher-order reflections being well-resolved, thus indicating excellent replication of SBA-15 into highly ordered 2D hexagonal Co_3O_4.

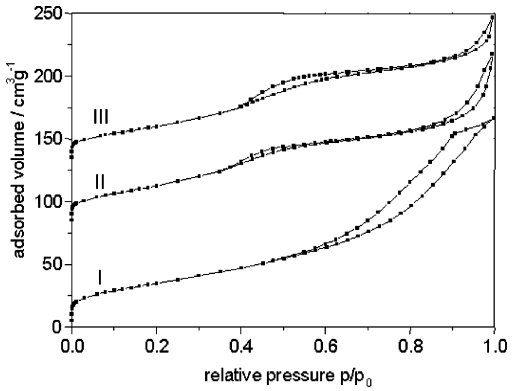

Figure 7. Nitrogen physisorption isotherms of nanocast Co_3O_4 obtained at different loadings. For clarity, measurements are plotted with an offset given in parentheses: (I) sample Co-Hex-100-15, (II) Co-Hex-100-18 (20 $cm^3\ g^{-1}$), and (III) Co-Hex-100-24 (40 $cm^3\ g^{-1}$).

Table 4. Nitrogen Physisorption Data from Nanocast Co_3O_4 as a Function of Loading[a]

sample	loading (%)	S_{BET} ($m^2\ g^{-1}$)	V_T ($cm^3\ g^{-1}$)	d_0 (nm)
Co-Hex-100-15	15	101	0.22	3.4
Co-Hex-100-18	18	122	0.16	5.1
Co-Hex-100-24	24	110	0.14	4.4

[a] BET surface areas, total pore volumes (V_T), and pore diameter (d_0) obtained from the desorption branch using the BJH algorithm.

Wide-angle XRD measurements confirm the formation of the Co_3O_4 spinel phase. Because of the low Si content of around 1% after the NaOH etching (EDX), formation of substantial amounts of Co_2SiO_4 can be excluded, and no evidence for such phases was found in any of the XRD patterns. Furthermore, from the wide-angle XRD, crystallite sizes can be calculated. For example, for the sample prepared at high loadings (Co-Hex-100-24), an average crystallite size of 16 nm (±1 nm) was estimated from the full width at half-maximum (fwhm) from all peaks in the 2θ range between 25 and 70° using the Scherrer equation. For the cubic spinel structure, application of the Scherrer formula results in the calculation of an equivalent spherical particle size ($V_{sphere} = 4/3\pi r^3$). Because the diameter of the cobalt oxide particles is known from the TEM, the length of crystallites along the nanowire axis can be calculated assuming cylindrical shapes ($V_{cylinder} = \pi r^2 h$) and a nanowire thickness of 7 nm (TEM). This calculation yields average domain lengths of 56 nm.

These results from TEM and XRD are supported by the data obtained with nitrogen physisorption measurements and SEM. Co-Hex-100-15 has a sorption isotherm with a broad capillary condensation range starting at about $p/p_0 = 0.6$ and extending almost to $p/p_0 = 1$, indicative of a high fraction of textural porosity (Figure 7). The pure Co_3O_4 samples, Co-Hex-100-18 and Co-Hex-100-24, gave a typical type IV isotherm with a clear H1-type hysteresis loop, which is characteristic for mesoporous materials. It is noticeable that the type of hysteresis clearly ressembles the hysteresis observed for highly ordered mesoporous carbon replica (CMK-3).[7]

Co-Hex-100-18 has a higher fraction of textural porosity than Co-Hex-100-24, also indicating larger ordered particles for the latter sample. Table 4 summarizes the textural data calculated from the isotherms.

The average length of Co_3O_4 wire bundles was determined from TEM to be around 400 nm for sample Co-Hex-100-18 and around 800 nm for sample Co-Hex-100-24. SEM images of the same three samples confirm that increasing domain sizes are present in Co_3O_4 samples with increasing loadings of cobalt oxide precursor (Figure 8). The morphology of sample Co-Hex-100-24 reflects the typical SBA-15 morphology, confirming the true replication. This characteristic morphology was not observed for sample Co-Hex-100-15.

The dependence of the morphology and the size of the ordered domains on precursor loading may appear evident on first sight. Nevertheless, the results prove that for a successful replication of the silica mold, loading is one of the crucial parameters, and they give a guideline in what range the loading should be adjusted. Zhao et al. used molar amounts of 6−10 mmol per g of porous silica in order to prepare Co_3O_4 using the nanocasting approach, which corresponds to a loading of 5−10% depending on the total pore volume of the parent silica. The amounts we used are several times higher than those described above, especially if the lower pore volumes of calcined samples compared to microwave-digested samples are taken into account. We could reproduce the preparation of nanocast Co_3O_4 using these lower loadings in microwave digested silica templates. However, the ordered domain sizes obtained were relatively small on the order of 50−100 nm. We note that we used a maximum loading of 30% Co_3O_4 in SBA-15, without the detection of bulk cobalt oxide particles outside of the pores of silica, as evidenced by TEM.

Reports in the literature and previous studies from our group have suggested that successful replication of Co_3O_4 is restricted to specific surface properties of the silica template.[20a] In this work, we succeeded in synthesizing nanocast Co_3O_4 from calcined SBA-15 and compared materials obtained from the calcined and the microwave-digested hard templates. This results in a substantial simplification and extends the range of available hard templates.

Figure 9 shows Co_3O_4 nanocast at different loadings from calcined (SBA-50-100-C1) and microwave-digested (SBA-50-100-MW) SBA-15 silica templates, respectively. As described above, a minimal loading of around 17% is necessary to achieve well-ordered materials if calcined silica hard templates are used. Lower loadings are sufficient for reasonably ordered arrays, if microwave-digested template silicas are used. The pictures show that earlier results[21] can be reproduced. The interconnectivity of the sample derived from silica SBA-50-100-MW is significantly higher for both loading values compared to the interconnectivity of the Co_3O_4 sample derived from SBA-50-100-C1, so that the cobalt oxide nanowires form ordered bundles at a loading of 14%. Nevertheless, at higher loading of 18%, the Co_3O_4 nanocast from the calcined template shows larger ordered domains compared to the material cast from microwave-digested silica. As illustrated in Figure 9, part IIb, a high amount of rather spherical ordered domains is formed in that case. These results are in line with the hypothesis that microwave-digested SBA-15 contains a complementary porosity in the walls of much larger dimensions, as we suggested above. With such mesoporous bridging connections in microwave-

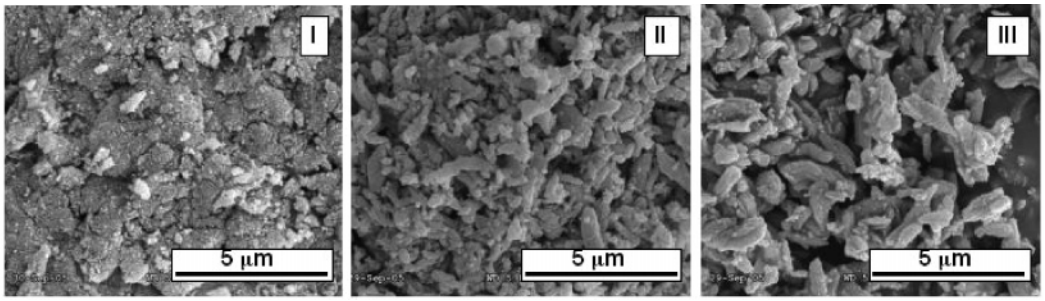

Figure 8. SEM images of nanocast Co_3O_4 obtained with different loadings of the cobalt oxide precursor. (I) Co-Hex-100-15, (II) Co-Hex-100-18, and (III) Co-Hex-100-24.

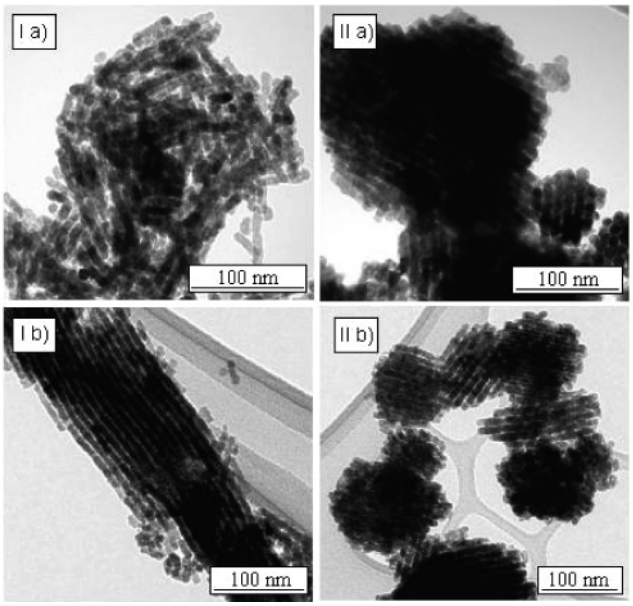

Figure 9. TEM images of nanocast Co_3O_4 with different loadings prepared from calcined SBA-15 ((Ia) 13 and (Ib) 18%) and from microwave-digested SBA-15 ((IIa) 14 and (IIb) 18%).

digested SBA-15, 3D accessibility can be assumed, which would favor the formation of spherical domains as opposed to the elongated nanowire bundles obtained from the calcined parent samples.

In spite of the fact that ordered Co_3O_4 can be synthesized with calcined parent silica, it seems probable that the higher concentration of surface silanol groups would lead to better interaction with the cobalt nitrate precursor. As mentioned above, microwave-digested SBA-15 has a smaller micropore volume than the calcined one. However, nanocasting with microwave-treated SBA-15 leads to ordered mesoporous metal oxides at lower loading. We suggest that this effect is mainly due to interconnecting bridges of larger diameters. Conditions during microwave digestion include high pressures and the presence of a corrosive medium used for chemical decomposition of the block copolymer template. This would, on the one hand, lead to an increased population of silanol groups on the walls and on the other hand, avoid pore shrinkage, which is related to the high temperatures during calcination. Figure 10 shows the isotherms of Co_3O_4 prepared with calcined and microwave-digested silica templates, respectively. For both samples, a type IV isotherm was observed. However, in both cases, the capillary condensation step is not very pronounced, indicative of relatively small sizes of ordered domains.

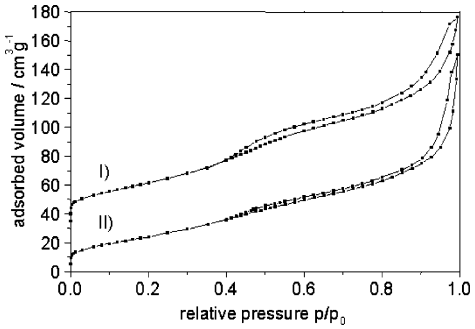

Figure 10. Nitrogen sorption isotherms of nanocast Co_3O_4 prepared from calcined SBA-50-100-C1 (I; offset of 30 cm^3 g^{-1}) and from microwave-digested SBA-50-100-MW (II) silica template.

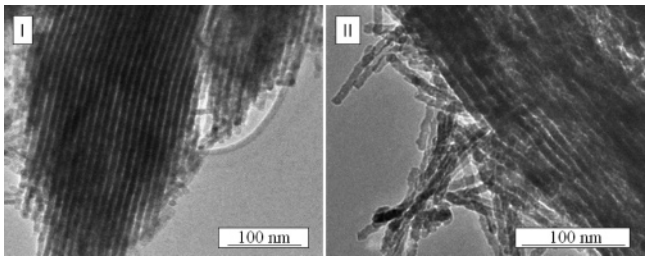

Figure 11. Interconnectivity and mesoporous ordered domain size. TEM images of nanocast Co_3O_4 depending on the SiO_2/P123 ratio of the parent SBA-15: SiO_2/P123 = 50 (I) and SiO_2/P123 = 60 (II).

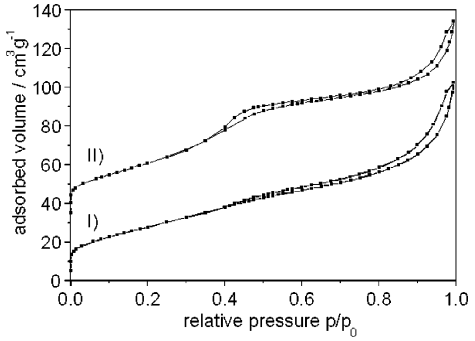

Figure 12. Nitrogen sorption isotherms of nanocast Co_3O_4 from SBA-60-100-C (I) and SBA-50-100-C1 (II; offset 30 cm^3 g^{-1}).

It has been reported that the density of porous connections between the mesoporous channels of SBA-15 is influenced by the temperature of the hydrothermal treatment during the preparation of SBA-15.[45] The network connectivity for different aging temperatures could be previously imaged by TEM using platinum replication.[17] A similar visualization of the network connectivity of bridging micropores for

(45) Kruk, M.; Jaroniec, M.; Ko, C. H.; Ryoo, R. *Chem. Mater.* **2000**, *12*, 1961.

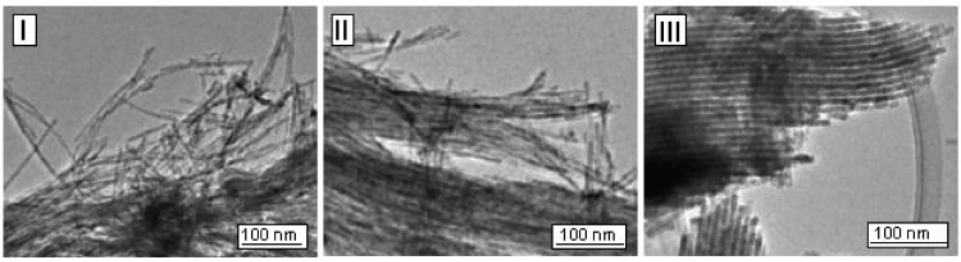

Figure 13. Effect of a size variation in 2D hexagonal parent silica on the nanocast Co_3O_4. TEM images of nanocast Co_3O_4: Co-Hex-50-30 (I), Co-Hex-80-30 (II), and Co-Hex-100-30 (III).

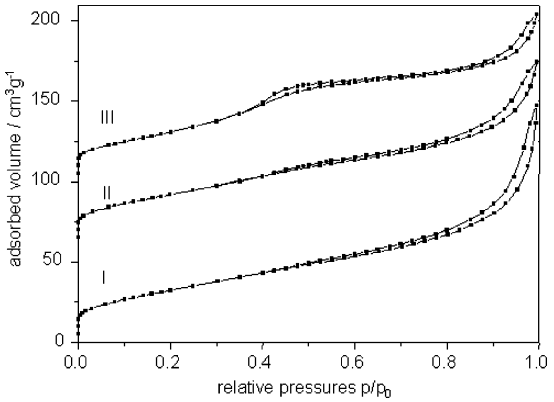

Figure 14. Nitrogen physisorption isotherms of Co_3O_4 nanocast from SBA-15 templates with different pore sizes with an offset given in parentheses: Co-Hex-50-30 (I), Co-Hex-80-30 (II, 60 $cm^3\ g^{-1}$), and Co-Hex-100-30 (III, 100 $cm^3\ g^{-1}$).

different SiO_2/P123 was also possible using replicated Co_3O_4 (Figure 11). After removal of silica with NaOH, nanocast Co_3O_4, which had been templated by SBA-15 prepared with a SiO_2/P123 molar ratio of 50, displays the ordered structure of SBA-15. In contrast, with SiO_2/P123 = 60, a smaller fraction of ordered domains could already be observed. For both samples, the same percentage of precursor loading was used relative to the pore volume of the parent SBA-15. The results from TEM are supported by nitrogen physisorption isotherms (Figure 12). For the Co_3O_4 sample nanocast from SBA-50-100-C1 (SiO_2/P123 = 50), a typical type IV isotherm with a H_1-type hysteresis was observed. In contrast to that, the isotherm of the Co_3O_4 sample prepared from SBA-60-100-C (SiO_2/P123 = 60) consists of both a small feature characteristic for the ordered mesopore system and the broad capillary filling range characteristic for textural porosity.

The preparation of well-ordered, mesoporous Co_3O_4 via nanocasting mainly depends on the template properties and the appropiate loading. Therefore, it should be possible to prepare different structures and sizes depending on the silica template. Hence, we used calcined SBA-15 and calcined KIT-6 with different pore diameters as templates for nanocast Co_3O_4, using an analogous procedure with high loadings as described above.

Pore diameters of both types of templates have been tuned by changing the temperature of hydrothermal treatment after the synthesis of the mesoporous silica. Other parameters, such as the silica to surfactant ratio (SiO_2/P123), were kept constant for all the templates. Figure 13 shows TEM images of Co_3O_4 nanocast from calcined SBA-15 of different pore diameters. As can be seen, it is possible to cast the mesopore structure from different SBA-15 silicas, resulting in Co_3O_4 nanowires of different diameters. Moreover, nanocasting using Co_3O_4 allows to image differences in network interconnectivity. All samples were prepared with the same loading. Nevertheless, Co_3O_4 nanocast from SBA-50-50-C (Co-Hex-50-30) does not contain ordered domains but well-separated long nanowires, whereas the sample nanocast from SBA-50-100-C1 (Co-Hex-100−30) predominantly features well-ordered 2D hexagonally ordered domains with Co_3O_4 arrays of nanowires reaching 1 μm in length. Co-Hex-80-30 represents an intermediate situation. Nitrogen physisorption supports the results from TEM, because only for sample Co-Hex-100-30 was a pronounced hysteresis observed,

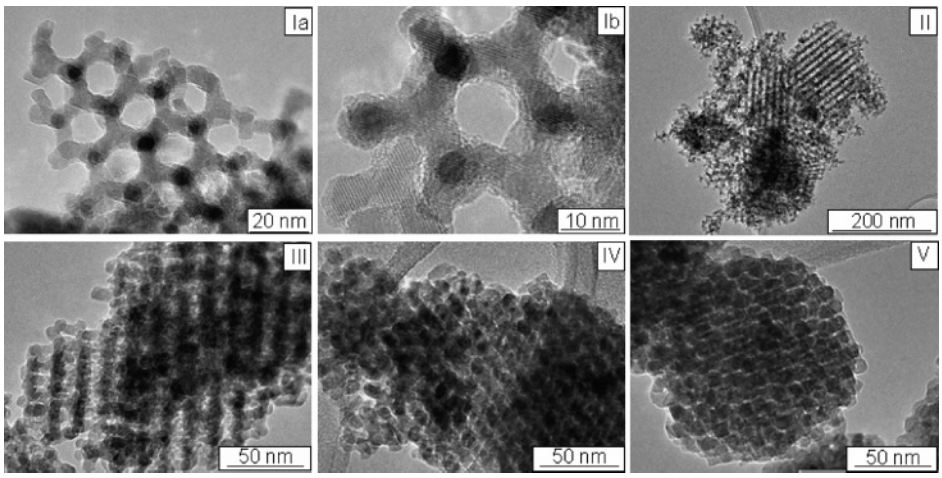

Figure 15. Effect of a size variation in 3D cubic parent silica on the nanocast Co_3O_4. TEM images of nanocast Co_3O_4: Co-Cubic-40-24 (Ia), Co-Cubic-40-11 (Ib), Co-Cubic-50-11 (II), Co-Cubic-80-24 (III), Co-Cubic-100-24 (IV), and Co-Cubic-135-24 (V).

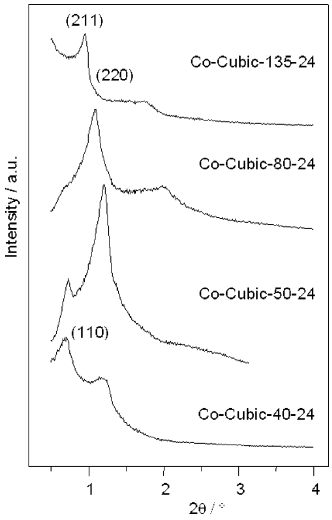

Figure 16. Powder XRD patterns for the cubic mesoporous Co_3O_4 from a series of cubic $Ia\bar{3}d$ KIT-6 synthesized at different temperatures of hydrothermal treatment.

characteristic of the mesoporous ordered domains (Figure 14).

In contrast to that, the pore system of KIT-6 is highly accessible and its replication with Co_3O_4 is expected to be facilitated with higher precursor loadings and higher interconnectivities compared to the use of SBA-15. Also, for cubic $Ia\bar{3}d$ silica materials, the nature of pore connectivity is influenced by the temperature of hydrothermal treatment.[34] We synthesized a series of cubic mesoporous Co_3O_4 from KIT-6 samples prepared at temperatures ranging from 40 to 135 °C. The quality of the cubic KIT-6 and its replicated Co_3O_4 was evaluated using nitrogen physisorption, powder XRD, and TEM.

As observed before from CMK-type carbon replication, lower aging temperatures during the preparation of KIT-6 may result in a decreased formation of interconnectivities within the gyroid structure.[34] For this reason, we suggest that two disconnected enantiomeric subframeworks within the parent silica are reflected in the Co_3O_4 nanocast from KIT-6 aged at lower temperatures.

Figure 15 shows representative TEM images of cubic mesoporous Co_3O_4 nanocast from KIT-6 that had been prepared at five different aging temperatures. The images clearly illustrate the effect of the size variation of the template on the resulting mesoporous Co_3O_4 materials. In the samples Co-Cubic-40-11 and Co-Cubic-50-11, uncoupled subframeworks could be observed on the edges with large-pore domains (Figure 15, parts Ia and Ib). Analogously to the uncoupled subframework of CMK-1,[45] this is an indication that the two pore systems of the parent template have not been interconnected with each other.

Powder XRD measurements at low angles show that a faithful replication of the cubic $Ia\bar{3}d$ symmetry was only preserved for the Co_3O_4 nanocast from KIT-6 synthesized at higher temperatures (Figure 16). When the parent KIT-6 was prepared at lower aging temperatures, the structure of the Co_3O_4 differs from the one with the $Ia\bar{3}d$ space group of the parent silica. The XRD pattern of the Co_3O_4 samples shows the narrow diffraction peak (211) with a half-width

Table 5. Physicochemical Properties of $Ia\bar{3}d$ Co_3O_4 as a Function of Parent KIT-6[a]

Co_3O_4	template	loading (%)	S_{BET} ($m^2\,g^{-1}$)	V_T ($cm^3\,g^{-1}$)	d_0 (nm)	D (nm)
Co-Cubic-40-11	KIT-40-C	11	152	0.47	11.1	4
Co-Cubic-50-11	KIT-50-C	11	134	0.41	10.8	5
Co-Cubic-80-24	KIT-80-C	24	111	0.30	10.9	7
Co-Cubic-100-24	KIT-100-C	24	113	0.20	8.5	8
Co-Cubic-135-24	KIT-135-C	24	83	0.1	5.1	10

[a] S_{BET} is the specific surface area of the nanocast Co_3O_4 deduced from the isotherm analysis in the relative pressure range of 0.05−0.2; V_T is the total pore volume at relative pressures 0.95; d_0 is the pore diameter of the Co_3O_4 calculated from the desorption branch of the isotherm using the BJH method; D is the wall thickness of Co_3O_4 determined from TEM analysis.

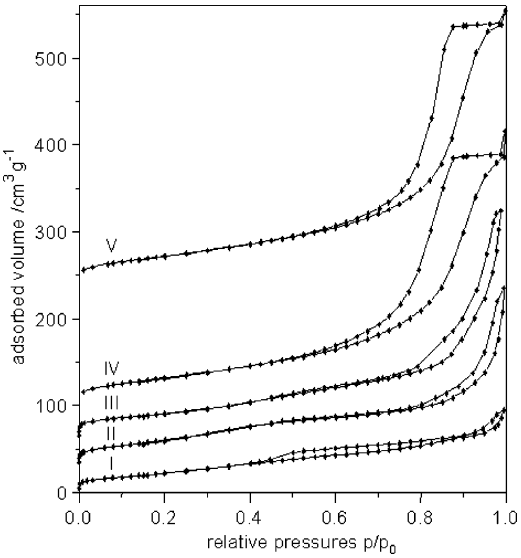

Figure 17. Nitrogen sorption isotherms of mesostructured Co_3O_4 samples obtained from different KIT-6 templates with an offset given in parentheses: Co-Cubic-135-24 (I), Co-Cubic-100-24 (II, 30 $cm^3\,g^{-1}$), Co-Cubic-80-24, (III, 60 $cm^3\,g^{-1}$), Co-Cubic-50-11 (IV, 90 $cm^3\,g^{-1}$) and Co-Cubic-40-11 (V, 230 $cm^3\,g^{-}$).

of about ±0.1° 2θ and the shoulder (220) indicating a high degree of ordering of the material. For the Co_3O_4 samples, which were nanocast from silica templates prepared at lower aging temperatures, a new reflection indexed as (110) is emerging in the low-angle range. Solovyov et al. described the appearance of an analogous reflection for CMK-1 materials and explained it by a lowering of the material symmetry because of a structural displacement.[43] Following this work, the reflection indexed as (110) can be assigned to the space group $I4_132$ characterizing the symmetry of a single Co_3O_4 subframework.

KIT-6 prepared at low aging temperatures, such as KIT-40-C and KIT-50-C, not only exhibits a marginal degree of interconnecting porosity but also features thick walls and small mesopore diameters. At high loadings of cobalt nitrate precursor (24%) in small mesopore silica, pore blocking and incidental formation of larger Co_3O_4 particles outside the mesoporous cubic $Ia\bar{3}d$ silica is facilitated. Therefore, the large pore Co_3O_4 nanocast from KIT-40-C and KIT-50-C was prepared at reduced loadings (11%). Table 5 shows that sample Co-Cubic-40-11 has a pore volume of 0.47 $cm^3\,g^{-1}$ and a BET surface area of 152 $m^2\,g^{-1}$. Figure 17 shows the nitrogen physisorption isotherms of the nanocast Co_3O_4 with different pore sizes. The isotherms indicate large mesopores for sample Co-Cubic-40-11. For this sample, the step due

to large mesopores merges with the sorption step due to textural porosity. For smaller pore Co_3O_4, such as sample Co-Cubic-135-24, these two steps could be better resolved.

The wall thicknesses of the silica templates, which are given in Table 2, are reflected in the pore sizes of the nanocast Co_3O_4 samples (Table 5). For samples Co-Cubic-40-11 and Co-Cubic-50-11, large pore diameters are found, also indicated by the capillary condensation step at high relative pressures. Using the BJH algorithm from the desorption branch of the nitrogen physisorption isotherms, a pore diameter of 11 nm was calculated; this corresponds to nearly twice the wall thickness of the parent silica material and indicates an initial low interconnectivity of the parent silica. It is a unique feature of these materials, that they have both large pores and high pore volumes, which may be important for a wide range of applications.

We have also used microwave digested KIT-6 as a hard template, but it was not possible to vary the wall thickness of the Co_3O_4 nanocast from these templates over such a wide range. Because of the smaller shrinkage effect of KIT-6 aged at lower temperatures during microwave digestion, the wall thickness of nanocast Co_3O_4 from those silica templates could be tuned only from 8 to 10 nm in this case (see the Supporting Information, Figure S5).

Conclusions

We have been able to synthesize ordered mesostructured Co_3O_4 networks from KIT-6 and SBA-15 mesoporous silicas of different pore sizes and systematically studied the dependence of the properties of the cobalt oxide on the nature of the parent silicas and the synthesis conditions. Depending on the interconnectivity of the SBA-15 silica host, loading of the cobalt oxide precursor and impregnation procedure, the structure of the resulting material could be tuned from randomly ordered rods of Co_3O_4 to fully interconnected mesoporous networks of nanowires with the same symmetry as the silica parent material. For tuning of the pore sizes and the shapes of the nanocast products, network interconnectivities of the parent silica and loading of the cobalt precursor are key parameters. Using an optimized and easy preparation procedure, it was possible to achieve loadings of Co_3O_4 inside the Co_3O_4/silica composite that are several times higher than those reported before.

Moreover, we compared in detail calcined silica hosts of different pore sizes with microwave-digested parent materials as a mold for Co_3O_4. With both templates, nanocasting of Co_3O_4 is possible, provided that the loading of the cobalt nitrate precursor in the parent silica matrix is appropriate and exceeds a certain threshold that depends on the nature of the mold. Although it is possible to avoid the microwave digestion and use calcined silica as the mold material, we confirmed that the preparation of well-ordered nanocast Co_3O_4 is facilitated if microwave-digested silica is used. The easier replication from microwave-digested SBA-15 is due to the formation of a higher fraction of interconnecting mesoporosity. Using the nanocasting approach, mesoscaled Co_3O_4 is accessible with a wide range of controllable textural and morphological properties. This expands the possibilities offered by this synthetic pathway and may make it adaptable to other metal precursors.

Acknowledgment. We thank B. Spliethoff and A. Dreier for TEM measurments, A. Bongard for SEM analysis, and Dr. C. Weidenthaler for particle determinations with XRD. F.K. thanks the Canadian Government for the Canada Research Chair on Functional Nanostructured Materials.

Supporting Information Available: Figures S1−S5. This material is available free of charge via the Internet at http://pubs.acs.org.

CM0610635